Yan-Ping Cao[1]
AML, Institute of Biomechanics and Medical Engineering,
Department of Engineering Mechanics,
Tsinghua University,
Beijing 100084, China
e-mail: caoyanping@tsinghua.edu.cn

Guo-Yang Li
AML, Institute of Biomechanics and Medical Engineering,
Department of Engineering Mechanics,
Tsinghua University,
Beijing 100084, China

Man-Gong Zhang
AML, Institute of Biomechanics and Medical Engineering,
Department of Engineering Mechanics,
Tsinghua University,
Beijing 100084, China

Xi-Qiao Feng
AML, Institute of Biomechanics and Medical Engineering,
Department of Engineering Mechanics,
Tsinghua University,
Beijing 100084, China

Determination of the Reduced Creep Function of Viscoelastic Compliant Materials Using Pipette Aspiration Method

Determining the mechanical properties of soft matter across different length scales is of great importance in understanding the deformation behavior of compliant materials under various stimuli. A pipette aspiration test is a promising tool for such a purpose. A key challenge in the use of this method is to develop explicit expressions of the relationship between experimental responses and material properties particularly when the tested sample has irregular geometry. A simple scaling relation between the reduced creep function and the aspiration length is revealed in this paper by performing a theoretical analysis on the aspiration creep tests of viscoelastic soft solids with arbitrary surface profile. Numerical experiments have been performed on the tested materials with different geometries to validate the theoretical solution. In order to incorporate the effects of the rise time of the creep pressure, an analytical solution is further derived based on the generalized Maxwell model, which relates the parameters in reduced creep function to the aspiration length. Its usefulness is demonstrated through a numerical example and the analysis of the experimental data from literature. The analytical solutions reported here proved to be independent of the geometric parameters of the system under described conditions. Therefore, they may not only provide insight into the deformation behavior of soft materials in aspiration creep tests but also facilitate the use of this testing method to deduce the intrinsic creep/relaxation properties of viscoelastic compliant materials.
[DOI: 10.1115/1.4027159]

Keywords: pipette aspiration test, reduced creep function, analytical analysis, finite element simulations

1 Introduction

Mechanical characterization of compliant materials (e.g., soft tissues, polymeric gels, and soft elastomers) is essential to many areas of science and engineering. For instance, in virtual surgery, realistic mechanical properties of soft tissues are required to build a reliable and interactive tissue model that provides the surgeons the skills that are difficult to learn from real patients [1]. In tissue engineering, the artificial soft tissues should have the mechanical properties similar to the real tissues in order to guarantee the mechanical compatibility [2]. Mechanical properties are also needed in understanding growth-induced deformation behavior of soft tissues as well as the responses of cells to various external stimuli [3–8]. Uniaxial tension, biaxial tension, and compression tests have been frequently used to measure the overall material properties. However, it is impossible or difficult to measure regional properties of compliant materials using these conventional testing methods. During past years, indentation tests [9–11], magnetic bead method [12,13], and the pipette aspiration method [14–23] have been frequently used to determine the mechanical properties of soft materials at a local area. This study is concerned with the aspiration creep tests of viscoelastic soft materials, in which the viscoelastic properties of soft materials could be measured by monitoring the variation of the aspiration length with time under given pressure [14,20,21]. When the geometries of both the pipette and the tested material are simple, e.g., the pipette is an ideal hollow cylinder, and the tested material can be assumed to be a half-space, analytical solutions are available to relate the material properties to the experimental responses [14,20,21]. Otherwise, the interpretation of the pipette aspiration tests may have to rely on the finite element simulations and the inverse analysis [22,24], which remains a challenging issue when the geometry of the tested material is irregular and/or the pressure imposed region is comparable to the size of the tested sample.

In this study, the pipette aspiration creep test of viscoelastic compliant materials (e.g., biological soft tissues, polymeric gels, and soft elastomers) is explored with the purpose to determine the *reduced* creep function. To this end, the following issues have been addressed: (1) the analytical solutions in the literature [14,20,21] to determine the creep function are applicable to the case where the pipette and the tested material have ideal geometries. Inspired by recent studies on the indentation of viscoelastic materials [25,26], it is expected that the geometric parameters of the system may play a negligible role in the determination of the reduced creep function under certain loading protocol. This issue is interesting and deserves systematic investigations. (2) The analytical solutions that permit evaluation of the creep function are established within the framework of linear elastic-viscoelastic theories. Previous studies [19,23,27] have demonstrated that the analytical solutions may contain significant errors when the deformation of the tested material is large. However, the critical deformation beyond which the linear elastic-viscoelastic theories are not applicable any more has not been clearly identified by investigating different hyperelastic material models and a broad material property range. (3) A linear relationship between the aspiration length l and the imposed pressure p forms the basis to derive the analytical solutions [14,20,21]. In a single pipette aspiration test, material, geometry, and boundary nonlinearities may be involved simultaneously, which can lead to a nonlinear $p - l$ relation. As aforementioned, effects of the material and geometric

[1]Corresponding author.

Manuscript received February 14, 2014; final manuscript received March 7, 2014; accepted manuscript posted March 13, 2014; published online April 1, 2014. Editor: Yonggang Huang.

nonlinearities have been demonstrated in the literature [19,23,27], to what extent the boundary nonlinearity affects the $p-l$ relation has not been carefully examined.

This paper is organized as follows. In Sec. 2, the definition of the reduced creep function and the importance to determine it are first discussed. We then reveal a simple scaling relation between the reduced creep function and the aspiration length based on dimensional analysis and elastic-viscoelastic correspondence principle. We show that this scaling relation is independent of the geometric parameters of both the pipette and the tested material provided that the $p-l$ relation is basically linear. Effects of the material, geometry, and boundary nonlinearities on the $p-l$ relation have been discussed in Sec. 3. The results on one hand establish the conditions under which the theoretical solution derived in Sec. 2 is valid, and on the other hand may guide the practical experimental setup. In Sec. 4, we validate and illustrate the usefulness of our results using numerical experiments. In Sec. 5, effects of the pressure rise time involved in the pipette aspiration creep tests have been explored and an analytical solution is derived to relate the aspiration length to the reduced creep function. The result is demonstrated to be useful by analyzing the experimental data from the literature. Section 6 gives the concluding remarks.

2 Theoretical Analysis

The creep function illustrated in Fig. 1(*a*) can be written in the following form: $J(t)=J(0)\tilde{J}$, where the instantaneous creep compliance $J(0)$ defines the elastic deformation behavior of the material. The reduced creep function $\tilde{J}(t)$ determines the intrinsic time-dependent deformation behavior of a linear viscoelastic soft material, which is the main concern of this study. For a generalized Maxwell model, the reduced creep function $\tilde{J}$ is usually written in the form of Prony series, i.e., $\tilde{J}(t)=1+\sum_{i=1}^{K} g_i[1-\exp(-t/\tau_i)]$, where t is the time, g_i and τ_i are material constants. When $\tilde{J}$ is known, the reduced relaxation function $\overline{E}$ may be determined using the relation of $\int_0^t \overline{E}(\xi)\tilde{J}(t-\xi)\,\mathrm{d}\xi = 2(1+v)t$. Either $\tilde{J}$ or $\overline{E}$ enables us to determine the loss factor [25,28], which is a key parameter measuring the damping property of viscoelastic compliant materials, e.g., soft tissues.

Our analysis starts from the pipette aspiration test of an elastic compliant material as shown in Fig. 1(*b*), and then adopts the elastic-viscoelastic correspondence principle [28] to deal with the test of viscoelastic materials. We assume that the geometries of the tested material and the pipette are arbitrary provided that the full contact between the aspiration tube end and the sample can be reached so that the negative pressure could be successfully imposed. The aspiration length, measuring the displacement of a point (e.g., point A in Fig. 1(*b*)) at the surface of the tested material, must be a function of the following independent parameters:

$$l = f(p, E, v, c_1, c_2, \ldots, c_M, d_1, d_2, \ldots, d_N) \tag{1}$$

where p is the imposed pressure, E and v are the elastic modulus and the Poisson's ratio of the tested material. The parameters $c_1, c_2, \ldots, c_M$ and $d_1, d_2, \ldots, d_N$ define the profile of the pipette and

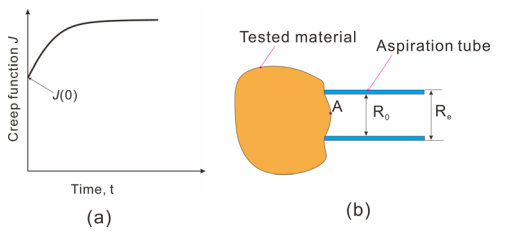

Fig. 1 (*a*) Schematic plot of the creep function; (*b*) illustration of the aspiration test, negative pressure is imposed to the surface of a tested material through a cylindrical tube with the inner radius R_0 and outer radius R_e

tested material, respectively, with M and N being finite integers. Dimensional analysis is adopted in this study, which states that a physical law does not depend on the arbitrariness in the choice of units of physical quantities [29]. Dimensional analysis has been frequently used to derive the relationships among the physical quantities involved in a physical process. For instance, it was first used in this way by Lord Rayleigh to understand why the sky is blue [30]. Here, we use this method to characterize the correlation between the experimental responses and the geometric and physical parameters of the system. Applying Buckingham Pi theorem in dimensional analysis [29] to Eq. (1) gives

$$l = c_1\Pi_0\left(\frac{p}{E}, v, \frac{c_2}{c_1^{\beta_2}}, \ldots, \frac{c_M}{c_1^{\beta_M}}, \frac{d_1}{c_1^{\gamma_1}}, \frac{d_2}{c_1^{\gamma_2}}, \ldots, \frac{d_N}{c_1^{\gamma_N}}\right) \tag{2}$$

where c_1 and E have the independent dimensions, β_K $(K=1,2,\ldots,M)$ and γ_L $(L=1,2,\ldots,N)$ are real numbers. c_1 has the length unit and may represent the inner radius R_0 of the pipette. Π_0 is a dimensionless function. Equation (2) represents a general expression of the $p-l$ curve for the pipette aspiration tests of a linear elastic material. The theory of linear elasticity predicts a linear relationship between p and l. Then, Eq. (2) can be further rewritten as

$$l = c_1\frac{p}{E}\Pi_{\mathrm{I}}\left(v, \frac{c_2}{c_1^{\beta_2}}, \ldots, \frac{c_M}{c_1^{\beta_M}}, \frac{d_1}{c_1^{\gamma_1}}, \frac{d_2}{c_1^{\gamma_2}}, \ldots, \frac{d_N}{c_1^{\gamma_N}}\right) \tag{3}$$

where Π_{I} is a dimensionless function. It is noticed that the linear relationship between the pressure and aspiration length has been used in previous studies [14,20,21] as well. In a practical pipette aspiration test, material, geometry, and boundary nonlinearities may be involved. Their effects will be addressed in Sec. 3, and the results may guide the experimental setup.

We then turn to the pipette aspiration tests of linear viscoelastic materials. Here, we focus on the case where the Poisson's ratio can be assumed as time independent, e.g., many soft tissues and elastomers are usually assumed to be incompressible with $v=0.5$. Invoking the elastic-viscoelastic correspondence principle [28,31], the $p-l$ relation can be obtained from Eq. (3) by replacing the elastic modulus E with $E^*(s)s$

$$\begin{aligned} l^*(s) &= c_1\frac{p^*(s)}{sE^*(s)}\Pi_{\mathrm{I}}\left(v, \frac{c_2}{c_1^{\beta_2}}, \ldots, \frac{c_M}{c_1^{\beta_M}}, \frac{d_1}{c_1^{\gamma_1}}, \frac{d_2}{c_1^{\gamma_2}}, \ldots, \frac{d_N}{c_1^{\gamma_N}}\right) \\ &= c_0 sJ^*(s)p^*(s)\Pi_{\mathrm{I}} \end{aligned} \tag{4}$$

where $E^*(s)$ and $J^*(s)$ are the Laplace transform of the relaxation modulus and the creep function, respectively, and s is the transform variable. $J^*(s)$ is related to $E^*(s)$ by $J^*(s)=1/(s^2E^*(s))$ [28]. $p^*(s)$ and $l^*(s)$ represent the Laplace transform of the pressure and the aspiration length, respectively. The elastic-viscoelastic correspondence principle was originally proposed for the problem for which the boundary conditions do not change with time. In pipette aspiration creep tests, the contact area between the aspiration tube and the tested material usually increases somehow during the creep procedure. We validate in Sec. 3 via finite element simulations that when the variation of the contact area is much smaller than the area of the pressure imposed region, the use of the correspondence principle is appropriate.

The inverse Laplace transform of Eq. (4) gives

$$l(t) = c_1\Pi_{\mathrm{I}}\int_0^t J(t-\tau)\mathrm{d}p \tag{5}$$

which can be further rewritten as

$$l(t) = c_1\Pi_{\mathrm{I}}\int_0^t J(t-\tau)\frac{\mathrm{d}p}{\mathrm{d}\tau}\mathrm{d}\tau \tag{6}$$

In a pipette aspiration creep test, the pressure may be described by the *Heaviside step function*.

$$p = \begin{cases} p = p_{\max} & (t \geq 0) \\ p = 0 & (t < 0) \end{cases} \tag{7}$$

where $p_{\max}$ is the creep pressure. The differential of the Heaviside step function gives the *Kronecker delta function*, and therefore inserting Eq. (7) into Eq. (6) gives

$$l(t) = c_1 \Pi_{\mathrm{I}} \int_0^t J(t-\tau) p_{\max} \delta(\tau) \mathrm{d}\tau \tag{8}$$

Based on the integral property of the Kronecker delta function, from Eq. (8) we have

$$l(t) = c_1 \Pi_{\mathrm{I}} p_{\max} J(t) \tag{9}$$

Equation (9) indicates that all the geometric parameters are included in the term of $c_1 \Pi_{\mathrm{I}}\left(\nu, \frac{c_2}{c_1^{\beta_2}}, \ldots, \frac{c_M}{c_1^{\beta_M}}, \frac{d_1}{c_1^{\gamma_1}}, \frac{d_2}{c_1^{\gamma_2}}, \ldots, \frac{d_N}{c_1^{\gamma_N}}\right)$, which is time independent. Equation (9) also gives $l(0) = c_1 \Pi_{\mathrm{I}} p_{\max} J(0)$, which together with Eq. (9) gives $l(t)/l(0) = c_1 \Pi_{\mathrm{I}} p_{\max} J(t)/(c_1 \Pi_{\mathrm{I}} p_{\max} J(0)) = J(t)/J(0)$, i.e.,

$$\tilde{J}(t) = \tilde{l}(t), \tag{10}$$

where $\tilde{l}(t) = l(t)/l(0)$. Here $l(0)$ represents the aspiration length at the starting point of the creep test. Equation (10) provides considerable insight into the deformation behavior of a viscoelastic compliant material in pipette aspiration creep tests. In particular it reveals that the evolution of the normalized aspiration length with time is determined by the reduced creep function and has nothing to do with other geometric and physical parameters. Equation (10) is supported by the analytical solution in the literature for the pipette and the tested material with simple geometries [14] and the main contribution made in this study is that we prove through the derivations above that Eq. (10) is a purely physical relation and independent of the geometric parameters of the system. In this sense, the reduced creep function can be determined from the normalized aspiration length using Eq. (10) even when the pipette and the tested material have irregular geometries. It is emphasized that the derivations above rely on a linear $p - l$ relation. In Sec. 3, we will investigate the effects of finite deformation and boundary nonlinearity on the relationship between p and l and establish the conditions under which a linear $p - l$ relation basically holds true.

3 Effects of Material, Geometry, and Boundary Nonlinearities on the $p - l$ Relation

The linear relationship between p and l during loading procedure forms the basis of the use of Boltzmann superposition and elastic-viscoelastic correspondence principle involved in previous studies [14,20,21] and this work. However, in practical loading and creep procedure, material, geometry, and boundary nonlinearities may be involved. It is therefore necessary and important to investigate their effects. Indeed, previous studies [19,23,27] have demonstrated the importance of considering the effects of finite deformation. In this study, we make an effort to determine the critical deformation below which a linear $p - l$ relation basically holds true. In a pipette aspiration test, the maximum effective strain in the tested material scales with the ratio the maximum aspiration length $l_{\max}$ to the size of the pressure imposed region, e.g., the pipette inner radius R_0. Therefore, $l_{\max}/R_0$ is used to measure the deformation in this study. To examine the effects of material nonlinearity, a nonlinear viscoelastic model implemented in ABAQUS [32] with viscous response characterized by a linear rate constitutive equation [33] is used in our finite element simulations. The initial elastic stored energy function in this model could have many choices [33]. Here, the strain energy functions for Mooney–Rivlin, Fung, and Arruda–Boyce hyperelastic models have been used as the initial elastic stored energy functions in the nonlinear viscoelastic equation [32,33]. In our simulations, the hyperelastic parameters in the Mooney–Rivlin [34,35], Fung [36], and Arruda–Boyce models [37], respectively, vary in a wide range. The fast loading procedure has been taken in which the loading time is much shorter than the characteristic relaxation time of the material. Finite element simulations give the $p - l$ curves. Our results show that the linear relationship between p and l basically holds true when $l_{\max}/R_0 \leq 0.3$; in this sense, the deformation corresponding to $l_{\max}/R_0 = 0.3$ may be regarded as the critical deformation beyond which the effects of material and geometric nonlinearities are significant. This conclusion is basically consistent with that drawn from the simulations of pipette aspiration of time-independent hyperelastic materials [38]. In principle, the solution proposed in this study is applicable to a free-standing soft film, but an additional condition of $l_{\max} \leq h$ is required considering the effects of finite rotation [39].

We then investigate the effects of boundary nonlinearity caused by the variation in the contact area between the pipette and the tested material. This important issue to the authors' knowledge has not been addressed in previous studies and examined in this study based on finite element simulations. Our results show that the effects of the contact area variation depend on the pipette wall thickness. Provided that the pipette wall thickness is much smaller than the pipette inner radius so that the ratio of contact area to the pressure imposed area is small, contact area variation has negligible effects on the linear relationship between p and l. But when the contact area between the pipette and the tested solid is not small in comparison with the area of the pressure imposed region and changes significantly during the loading and creep procedure, the $p - l$ relation is not linear any more even when the deformation of the tested material is small. Figure 2 represents critical examples illustrating this issue, in which the pipette has geometric defects, i.e., the end of the pipette is nonflat. Three cases are explored where the pipette wall thicknesses are different, and the initial line contact between the pipette and the tested material changes to the surface contact during the loading and creep procedure, Fig. 2. The maximum contact area decreases from case I to case III, and in case III it is much smaller than the pressure imposed area. Figure 3 represents the identified reduced creep function using Eq. (10) for different cases, which indicates that Eq. (10) is pretty accurate provided the variation in the contact area is much smaller than the pressure imposed area. Based on the discussions above, it is suggested to adopt a thin wall pipette in practical experiments to deduce the reduced creep function using Eq. (10) considering the effects of boundary nonlinearity in particular when the tested material has irregular shape and/or the pipette has geometry defects.

4 Numerical Experiments

Numerical experiments are carried out to illustrate the usefulness of the scaling relation given by Eq. (10). Using a general purpose finite element software, ABAQUS [32], we simulate the pipette aspiration creep tests of the samples with different profiles as shown in Fig. 4. In our simulations, the instantaneous modulus E is taken as 2 MPa, and the Poisson's ratio $\nu = 0.48$. Both traction-free and fixed boundary conditions are explored. In the simulations, the effects of finite deformation have been included. Four axisymmetric examples are studied here for the sake of simplicity of simulations though our theoretical analysis does not have this restriction. In these examples, the two conditions identified in Sec. 3, i.e., $l_{\max}/R_0 \leq 0.3$ and the variation in the contact area is much smaller than the pressure imposed area, are satisfied under which the effects of finite deformation and boundary nonlinearity are negligible and the $p - l$ relation is basically linear.

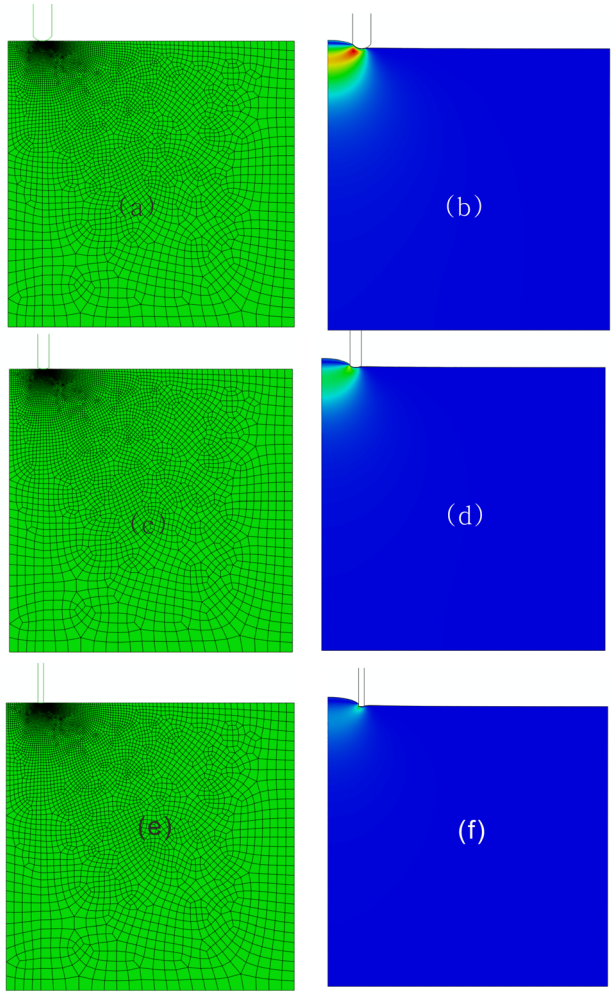

Fig. 2 Finite element models used to examine the effects of the variation in the contact area on the identified reduced creep function using Eq. (10). (*a*) and (*b*) represent the computational model and the deformation of the tested material for case I; (*c*) and (*d*) represent the computational model and the deformation of the tested material for case II; (*e*) and (*f*) are the computational model and the deformed configuration of the tested material for case III.

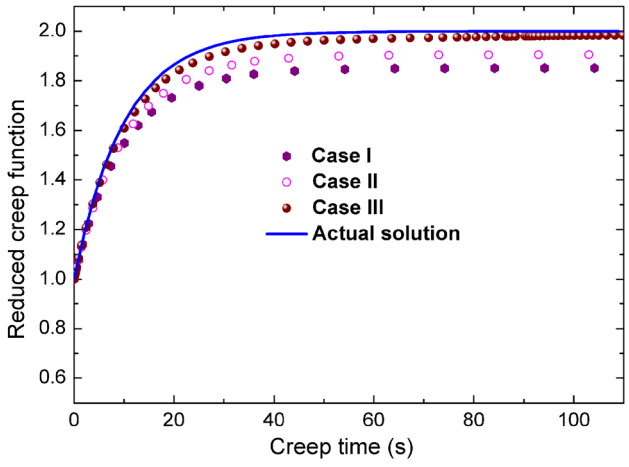

Fig. 3 A comparison of the identified reduced creep functions using Eq. (10) with the actual solution input in the finite element simulations: $\bar{J}(t) = 1 + (1 - \exp(-t/10))$ for different cases

4.1 Example A. We first consider a pipette aspiration creep test of a viscoelastic half-space, where the inner pipette radius R_0 is much smaller than the size of the tested soft material. Figure 4(*a*) illustrates the computational model. A total of 4947 eight-node quadrilateral axisymmetric elements are used to model the substrate. The creep pressure is taken as $p_{max} = 0.3$ MPa. Figure 4(*b*) presents the deformed configuration. The ratio of l_{max}/R_0 is around 0.25 in this example, where l_{max} is the maximum aspiration length. A_1 in Fig. 4(*a*) is fixed to eliminate the rigid-body motion in the simulations.

4.2 Example B. This example dedicates to verify the applicability of Eq. (10) to the circumstances under which the tested solid is not a flat half-space and its size is comparable with the pipette inner radius. The axisymmetric computational model is given by Fig. 4(*c*). To model the tested material, 2137 eight-node quadrilateral axisymmetric elements are used. The creep pressure is taken as $p_{max} = 0.15$ MPa. The maximum aspiration length is around 0.16 R_0 in this example, and the corresponding deformed configuration is presented in Fig. 4(*d*).

4.3 Example C. In this example, we explore a pipette aspiration creep test of a free-standing film. The computational model is given by Fig. 4(*e*) and a total of 3630 eight-node quadrilateral axisymmetric elements are used to model the soft film. Since the pipette inner radius is comparable with the film thickness, the tested solid cannot be assumed as a half-space. The creep pressure is taken as $p_{max} = 0.15$ MPa. Figure 4(*f*) presents the deformed configuration of the film and the ratio of l_{max}/R_0 in this example is 0.29.

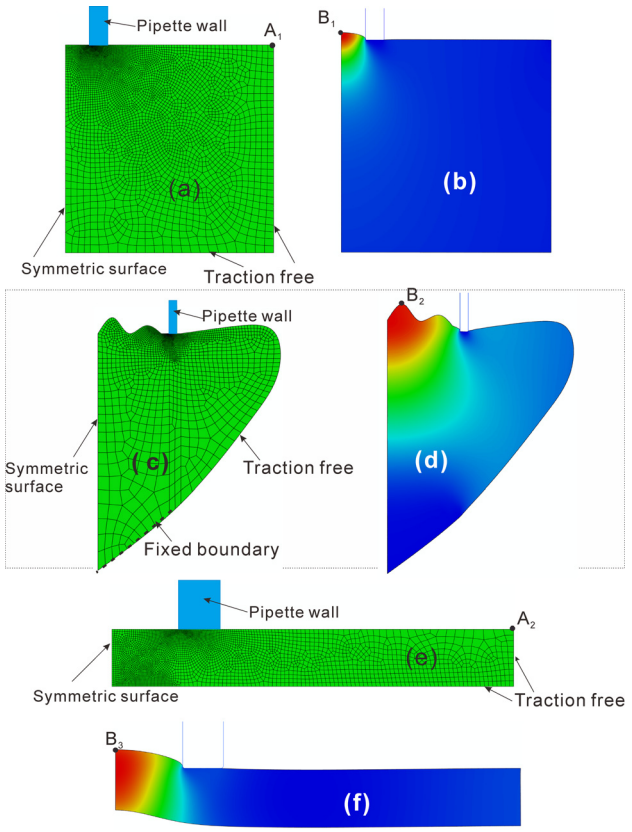

Fig. 4 Numerical experiments used to illustrate the usefulness of the analytical solution given by Eq. (10). (*a*), (*c*), and (*e*) represent the finite element models for examples A, B, and C, respectively. A_1 and A_2 in (*a*) and (*c*) are fixed to eliminate the rigid-body motion of the tested materials, other points can be selected which has on effects on the identified results. (*b*), (*d*), and (*f*) are the deformed configurations. The displacements at $B_i (i = 1, 2, 3)$ are recorded as the aspiration lengths.

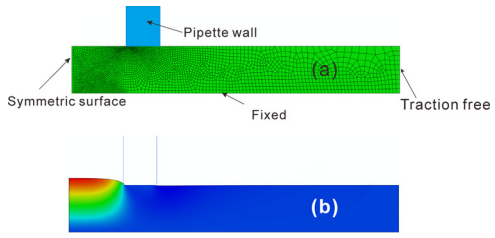

Fig. 5 Pipette aspiration test of soft layer bonded to rigid substrate. (*a*) Finite element model; (*b*) deformed configuration of the tested material, the displacement at the center point of the upper surface is recorded as the aspiration length.

4.4 Example D. Finally, we consider a pipette aspiration creep test of a viscoelastic soft layer bonded on a rigid substrate as shown in Fig. 5. This example is different from the example **C** at the boundary condition. In this example, the bottom is fixed instead of traction free. With the increase in the aspiration length, the effect of the rigid substrate on the $p-l$ relation will come into play. Theoretical analysis in Sec. 2 shows that Eq. (10) is applicable for this problem. The creep pressure is taken as $p_{\max}=0.3$ MPa. Figure 5(*b*) presents the deformed layer under $l_{\max}/R_0=0.12$.

For all the examples above, the variation of the aspiration length with time in the creep procedure is recorded, which gives the $\tilde{l}(t)$. Then, the reduced creep function $\tilde{J}(t)$ is determined from Eq. (10) and plotted in Fig. 6 (points). The actual $\tilde{J}(t)$ used as the input in our finite element analysis is included in Fig. 6 for comparison (lines). Figure 6 indicates that indeed Eq. (10) is basically geometric independent and applicable to the case where the tested material has irregular shape and/or the size of the specimen is comparable with that of the pressure imposed area provided that the conditions identified in Sec. 3 are satisfied. But it should be pointed out that the effects of finite deformation appear to be more pronounced in Example D in comparison with other examples.

5 Interpreting the Experimental Data by Incorporating the Effects of the Pressure Rise Time

In the theoretical analysis in Sec. 2, the creep pressure is described with a Heaviside step function as given by Eq. (7). However, in practical pipette aspiration creep tests, it takes time for the pressure to reach the imposed value. This time period is here named as the pressure rise time t_r, and illustrated in Fig. 7(*a*)

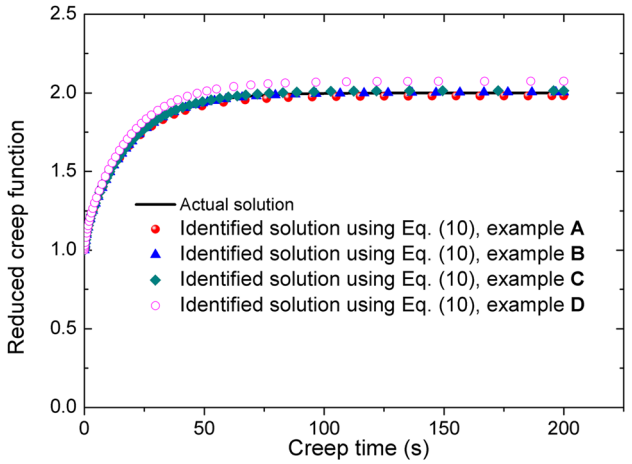

Fig. 6 A comparison of the identified reduced creep functions using Eq. (10) and the aspiration lengths given by finite element simulations with the actual solution. The actual solution is taken here as $\tilde{J}(t)=1+0.1(1-\exp(-t))+0.9(1-\exp(-t/18))$. Here, the actual solution represents the reduced creep function input in the finite element simulations.

as well. Provided that t_r is much shorter than the characteristic relaxation time of the tested material, its effects are negligible but it may play a role when it is not small. Merryman et al. [20] have incorporated Boltzmann superposition into the half-space model to account for effects of pressure rise time. We here derived a theoretical solution based on Eq. (6) for a viscoelastic material with arbitrary profile and described by the generalized Maxwell model (Fig. 7(*b*)) to incorporate the effects of t_r. The creep function for the generalized Maxwell model may be written in the form of a Prony series

$$J(t)=J(0)\left(1+\sum_{i=1}^{K}g_i[1-\exp(-t/\tau_i)]\right) \tag{11}$$

where g_i and τ_i $(i=1,2,3)$ are material constants. The reduced creep function in this case is $\tilde{J}(t)=1+\sum_{i=1}^{K}g_i[1-\exp(-t/\tau_i)]$. For the loading procedure illustrated in Fig. 7(*a*), inserting Eq. (11) into Eq. (6) leads to the following relation:

$$\tilde{l}(t)=\frac{1+\sum_{i=1}^{K}g_i(1-\Phi_i\exp(-t/\tau_i))}{1+\sum_{i=1}^{K}g_i(1-\Phi_i\exp(-t_r/\tau_i))}\quad(t\geq t_r) \tag{12}$$

where $\Phi_i=(\tau_i/t_r)[\exp(t_r/\tau_i)-1]$, is an affecting factor depending on the ratio of material time constants to the pressure rise time t_r. Again, Eq. (12) is independent of the geometry of the system. $t_r\to 0$ leads to $\Phi_i\to 1$, and under this circumstance Eq. (12) reduces to Eq. (10), i.e., $\tilde{l}(t)=1+\sum_{i=1}^{K}g_i[1-\exp(-t/\tau_i)]$. Here, we focus on the widely used standard linear solid model (Zener model) [28]. In this case, Eq. (12) reduces to the following form:

$$\tilde{l}(t)=\frac{1+g_1(1-\Phi_1\exp(-t/\tau_1))}{1+g_1(1-\Phi_1\exp(-t_r/\tau_1))}\quad(t\geq t_r) \tag{13}$$

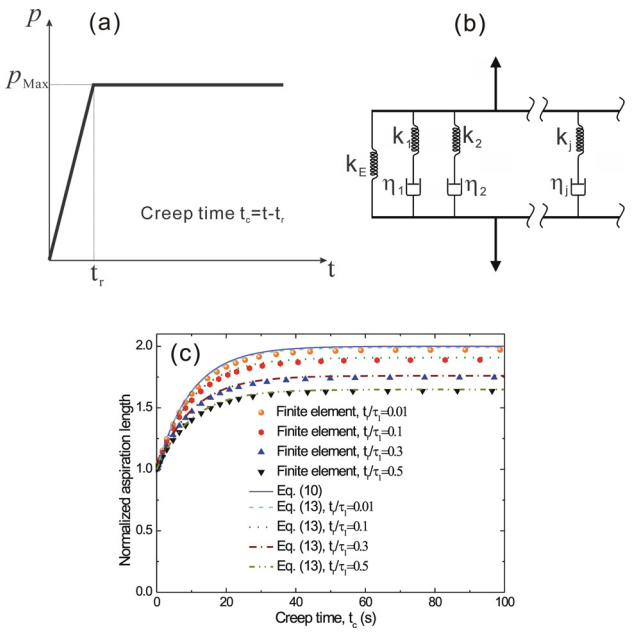

Fig. 7 (*a*) Illustration of the loading procedure in an aspiration creep test, where t_r is the time at which the negative pressure reach the maximum value and then is kept as constant; (*b*) schematic plot of the generalized Maxwell model, where $K_e, K_1, K_2, \ldots, K_j$ are spring constants and $\eta_1, \eta_2, \ldots, \eta_j$ are viscosity coefficients; (*c*) normalized aspiration lengths given by finite element simulations and those predicted using Eqs. (10) and (13)

where $\Phi_1 = \tau_1/t_r[\exp(t_r/\tau_1) - 1]$, τ_1 is the characteristic relaxation time of the tested material. Consider the example shown in Fig. 4(*a*), finite element simulations are carried out to determine $\tilde{l}(t)$ for the Zener model with $g_1 = 1$ and $\tau_1 = 10$ s. $\tilde{l}(t)$ given by the finite element analysis and those predicted using Eqs. (10) and (13) are plotted in Fig. 7(*c*) for different ratios of t_r/τ_1. This plot indicates that Eq. (10) is pretty accurate when $t_r/\tau_1 << 1$. When t_r is comparable to the material time constant, Eq. (12) or Eq. (13) should be used for determining $\tilde{J}(t)$. To further illustrate the usefulness of Eqs. (12) and (13), we analyse the experimental data reported in the study of Merryman et al. [20]. Figure 8(*a*) represents the variation of the aspiration length with loading and creep time. The experimental data given in Fig. 8(*a*) permits determination of $\tilde{l}(t)$ as given in Fig. 8(*b*). Using the Zener model to describe $\tilde{J}(t)$, Fig. 8(*b*) and Eq. (10) give the material constants $\tau_1 = 15$ s and $g_1 = 3.75$. τ_1 and g_1 determined using Eq. (13) and Fig. 8(*b*) are $\tau_1 = 15$ s, and $g_1 = 6$, respectively, where $t_r = 2.5$ s following Merryman et al. [20]. The above results indicate that Eq. (10) underestimates the parameter g_1 when the pressure rise time is not much smaller than material relaxation time. It is emphasized here that in the use of both Eqs. (10) and (13), the knowledge on the geometric parameters of the system is not required. The experimental result is used here to illustrate the importance to consider the pressure rise time in Eq. (13). Provided that the experiment suffers from the effects of the boundary nonlinearity and the finite deformation of the tested material, the estimated material constants may contain significant errors.

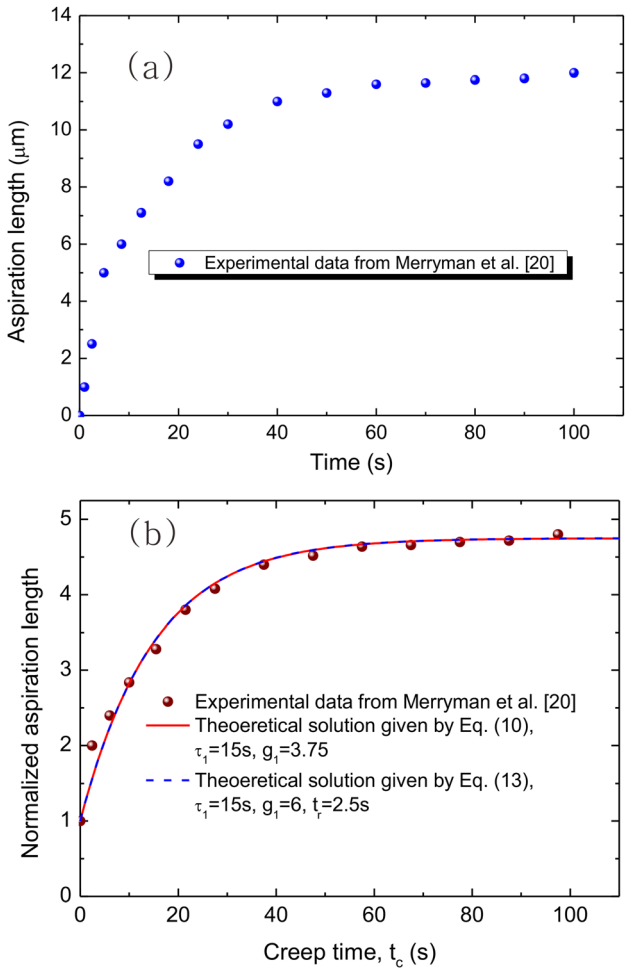

Fig. 8 Experimental data used to illustrate the difference between the result identified using Eq. (10) and that given by Eq. (13). (*a*) Variation of the aspiration length with time given by the experiments of Ref. [20]; (*b*) normalized aspiration length $\tilde{l}(t)$ at the creep stage.

6 Concluding Remarks

In this study, we have explored the pipette aspiration creep tests of compliant materials for determining the reduced creep function $\tilde{J}(t)$, which defines the intrinsic creep/relaxation behavior of a linear viscoelastic material. In summary, the following contributions have been made.

First, our theoretical analysis based on dimensional analysis and elastic-viscoelastic correspondence principle leads to a simple scaling relation between the reduced creep function and the normalized aspiration length, i.e., $\tilde{J}(t) = \tilde{l}(t)$. We prove that this scaling relation is independent of the geometric parameters of the system provided that the $p - l$ relation is basically linear. Therefore, the analysis and the solution reported here are particularly useful for determining the reduced creep function when the tested material has irregular profile and/or the pipette is not an ideal cylindrical tube.

Second, effects of material, geometry, and boundary nonlinearities on the $p - l$ relation are examined. The conditions under which a linear relationship between p and l exists have been established. In this study, the ratio of $l_{\max}/R_0$, which scales with the maximum effective strain in the tested material, is used to measure the effects of the material and geometry nonlinearities. Our results show that the effects of the material and geometry nonlinearities are negligible when $l_{\max}/R_0 \leq 0.3$. This conclusion indicates that the analytical solutions in the literature [14,20,21] and those obtained in this work may be of limited use when the size of the tested material is very small, e.g., soft microparticles. In this case, a measurable $l_{\max}$ may be comparable or even greater than R_0. However, the analytical solution obtained in this study may find wide applications in the testing of some biological soft tissues, e.g., livers and kidneys, and the compliant artificial materials at macroscale, where the condition of $l_{\max}/R_0 \leq 0.3$ can be easily satisfied by taking an appropriate R_0. Effects of boundary nonlinearity strongly depend on the contact area and its variation. If the contact area between the pipette and the tested material is not small in comparison with the pressure imposed region and its variation is significant during the test, the $p - l$ relation can be nonlinear even when the deformation is small. Based on this finding, we suggest the use of a thin wall pipette when adopting the analytical solution reported in this study to measure the reduced creep function, which could effectively avoid or alleviate the nonlinearity introduced by the variation in the contact area.

Third, considering that it takes time for the pressure to reach the maximum value in a pipette aspiration creep test and the Heaviside step function is an approximation of the practical loading procedure, analytical solutions (Eqs. (12) and (13)) are derived to incorporate the effects of the pressure rise time. The usefulness of Eqs. (12) and (13) has been demonstrated using a numerical example and the analysis of the experimental data from literature. We show that the analytical solutions given by Eqs. (12) and (13) are independent of the geometric parameters of the system as well. Therefore, they can be used in the case where the pipette is not a cylindrical tube and/or the tested material can not be assumed as a half-space.

The analysis and the findings in this study should help understand the pipette creep test and facilitate the use of this testing method to characterize the mechanical properties of time-dependent compliant materials. It is worth emphasis that this study is limited to the determination of the reduced creep function. Writing the creep function in the form of $J(t) = J(0)\tilde{J}$, the *creep* function $\tilde{J}$ defines the intrinsic time-dependent deformation behavior of viscoelastic materials. We show that the determination of $\tilde{J}$ does not require the knowledge of the geometric parameters if the $p - l$ relation is linear. However, this conclusion is not applied to the determination of $J(0)$, which cannot be obtained from the analytical solutions proposed here. Besides, this study is concerned with the pipette aspiration of viscoelastic compliant materials. Viscoelasticity and poroelasticity commonly coexist as

time-dependent behaviors in some soft materials, e.g. polymer gels. Very recently, Wang et al. [40] have proposed a method capable of separating viscoelasticity and poroelasticity of gels in various mechanical tests. Their method may help understand the pipette aspiration of polymer gels when poroelastic properties are the main concern and this issue deserves further investigation.

Acknowledgment

Support from the National Natural Science Foundation of China (Grant No. 11172155), Tsinghua University and 973 Program of MOST (2010CB631005) is gratefully acknowledged.

References

[1] Ahn, B., and Kim, J., 2010, "Measurement and Characterization of Soft Tissue Behavior With Surface Deformation and Force Response Under Large Deformations," Med. Image Anal., **14**(2), pp. 138–148.
[2] Wang, M., 2003, "Developing Bioactive Composite Materials for Tissue Replacement," Biomaterials, **24**(13), pp. 2133–2151.
[3] Desprat, N., Richert, A., Simeon, J., and Asnacios, A., 2005, "Creep Function of a Single Living Cell," Biophys. J., **88**(3), pp. 2224–2233.
[4] Discher, D. E., Janmey, P., and Wang, Y. L., 2005, "Tissue Cells Feel and Respond to the Stiffness of Their Substrate," Science, **310**(5751), pp. 1139–1143.
[5] Butcher, J. T., McQuinn, T. C., Sedmera, D., Turner, D., and Markwald, R. R., 2007, "Transitions in Early Embryonic Atrioventricular Valvular Function Correspond With Changes in Cushion Biomechanics That are Predictable by Tissue Composition," Circ. Res., **100**(10), pp. 1503–1511.
[6] Vaziri, A., and Gopinath, A., 2008, "Cell and Biomolecular Mechanics in Silico," Nat. Mater., **7**(1), pp. 15–23.
[7] Lv, S., Dudek, D. M., Cao, Y., Balamurali, M. M., Gosline, J., and Li, H., 2010, "Designed Biomaterials to Mimic the Mechanical Properties of Muscles," Nature, **465**(7294), pp. 69–73.
[8] Li, B., Cao, Y. P., Feng, X. Q., and Gao, H., 2012, "Mechanics of Morphological Instabilities and Surface Wrinkling in Soft Materials: A Review," Soft Matter, **8**(21), pp. 5728–5745.
[9] Cheng, Y. T., and Cheng, C. M., 2004, "Scaling, Dimensional Analysis, and Indentation Measurements," Mater. Sci. Eng. R-Rep., **44**(4–5), pp. 91–149.
[10] Kranenburg, J. M., Tweedie, C. A., van Vliet, K. J., and Schubert, U. S., 2009, "Challenges and Progress in High—Throughput Screening of Polymer Mechanical Properties by Indentation," Adv. Mater., **21**(35), pp. 3551–3561.
[11] Oyen, M. L., 2007, "Sensitivity of Polymer Nanoindentation Creep Measurements to Experimental Variables," Acta Mater., **55**(11), pp. 3633–3639.
[12] Smith, S. B., Finzi, L., and Bustamante, C., 1992, "Direct Mechanical Measurements of the Elasticity of Single DNA Molecules by Using Magnetic Beads," Science, **258**(5085), pp. 1122–1126.
[13] Ziemann, F., Rädler, J., and Sackmann, E., 1994, "Local Measurements of Viscoelastic Moduli of Entangled Actin Networks Using an Oscillating Magnetic Bead Micro-Rheometer," Biophys. J., **66**(6), pp. 2210–2216.
[14] Sato, M., Theret, D. P., Ohshima, N., Nerem, R. M., and Wheeler, L. T., 1990, "Application of the Micropipette Technique to the Measurement of Cultured Porcine Aortic Endothelial Cell Viscoelastic Properties," ASME J. Biomech. Eng., **112**(3), pp. 263–268.
[15] Discher, D. E., Mohandas, N., and Evans, E. A., 1994, "Molecular Maps of Red Cell Deformation: Hidden Elasticity and In Situ Connectivity," Science, **266**(5187), pp. 1032–1035.
[16] Aoki, T., Ohashi, T., Matsumoto, T., and Sato, M., 1997, "The Pipette Aspiration Applied to the Local Stiffness Measurement of Soft Tissues," Ann. Biomed. Eng., **25**(3), pp. 581–587.
[17] Hochmuth, R. M., 2000, "Micropipette Aspiration of Living Cells," J. Biomech., **33**(1), pp. 15–22.
[18] Trickey, W. R., Lee, G. M., and Guilak, F., 2000, "Viscoelastic Properties of Chondrocytes From Normal and Osteoarthritic Human Cartilage," J. Orthop. Res., **18**(6), pp. 891–898.
[19] Zhou, E. H., Lim, C. T., and Quek, S. T., 2005, "Finite Element Simulation of the Micropipette Aspiration of a Living Cell Undergoing Large Viscoelastic Deformation," Mech. Adv. Mater. Struct., **12**(6), pp. 501–512.
[20] Merryman, W. D., Guilak, F., Sacks, M. S., and Bieniek, P. D., 2009, "Viscoelastic Properties of the Aortic Valve Interstitial Cell," ASME J. Biomech. Eng., **131**(4), p. 041005.
[21] Guevorkian, K., Colbert, M. J., Durth, M., Dufour, S., and Brochard-Wyart, F. 2010, "Aspiration of Biological Viscoelastic Drops," Phys. Rev. Lett., **104**(21), p. 218101.
[22] Zhao, R., Sider, K. L., and Simmons, C. A., 2011, "Measurement of Layer-Specific Mechanical Properties in Multilayered Biomaterials by Micropipette Aspiration," Acta Biomater., **7**(3), pp. 1220–1227.
[23] Zhou, E. H., Xu, F., Quek, S. T., and Lim, C. T., 2012, "A Power-Law Rheology-Based Finite Element Model for Single Cell Deformation," Biomech. Model Mech., **11**(7), pp. 1075–1084.
[24] Zhao, R., Wyss, K., and Simmons, C. A., 2009, "Comparison of Analytical and Inverse Finite Element Approaches to Estimate Cell Viscoelastic Properties by Micropipette Aspiration," J. Biomech., **42**(16), pp. 2768–2773.
[25] Cao, Y. P., Ji, X. Y., and Feng, X. Q., 2010, "Geometry Independence of the Normalized Relaxation Functions of Viscoelastic Materials in Indentation," Philos. Mag., **90**(12), pp. 1639–1655.
[26] Cao, Y. P., Zhang, M. G., and Feng, X. Q., 2013, "Indentation Method for Measuring the Viscoelastic Kernel Function of Nonlinear Viscoelastic Soft Materials," J. Mater. Res., **28**(6), pp. 806–816.
[27] Baaijens, F. P., Trickey, W. R., Laursen, T. A., and Guilak, F., 2005, "Large Deformation Finite Element Analysis of Micropipette Aspiration to Determine the Mechanical Properties of the Chondrocyte," Ann. Biomed. Eng., **33**(4), pp. 494–501.
[28] Lakes, R. S., 2009, *Viscoelastic Materials*, Cambridge University Press, New York.
[29] Barenblatt, G. I., 1996, *Scaling, Self-Similarity, and Intermediate Asymptotics: Dimensional Analysis and Intermediate Asymptotics*, Cambridge University Press, New York.
[30] Pesic, P., 2005, *Sky in a Bottle*, MIT, Cambridge, MA.
[31] Christensen, R. M., 1982, *Theory of Viscoelasticity: An Introduction*, Academic, New York.
[32] DS Simulia Corp., 2010, "ABAQUS User's Manual," Version 6.10, Dassault Systemes, Providence, RI.
[33] Simo, J. C., 1987, "On a Fully Three-Dimensional Finite-Strain Viscoelastic Damage Model: Formulation and Computational Aspects," Comput. Meth. Appl. Mech. Eng., **60**(2), pp. 153–173.
[34] Mooney, M., 1940, "A Theory of Large Elastic Deformation," J. Appl. Phys., **11**(9), pp. 582–592.
[35] Rivlin, R. S., 1948, "Large Elastic Deformations of Isotropic Materials. IV. Further Developments of the General Theory," Philos. Trans. R. Soc., A, **241**(835), pp. 379–397.
[36] Fung, Y. C., Fronek, K., and Patitucci, P., 1979, "Pseudoelasticity of Arteries and the Choice of Its Mathematical Expression," Am. J. Physiol., **237**(5), pp. H620–H631.
[37] Arruda, E. M., and Boyce, M. C., 1993, "A Three-Dimensional Constitutive Model for the Large Stretch Behavior of Rubber Elastic Materials," J. Mech. Phys. Solids, **41**(2), pp. 389–412.
[38] Zhang, M. G., Cao, Y. P., Li, G. Y., and Feng, X. Q., "Pipette Aspiration of Hyperelastic Compliant Materials: Theoretical Analysis, Simulations, and Experiments" (unpublished).
[39] Chien, W. Z., 1947, "Large Deflection of a Circular Clamped Plate Under Uniform Pressure," Acta Phys. Sin., **7**(2), pp. 102–107.
[40] Wang, Q. M., Mohan, A. C., Oyen, M. L., and Zhao, X. H., 2014, "Separating Viscoelasticity and Poroelasticity of Gels With Different Length and Time Scales," Acta Mech. Sin., **30**(1), pp. 20–27.